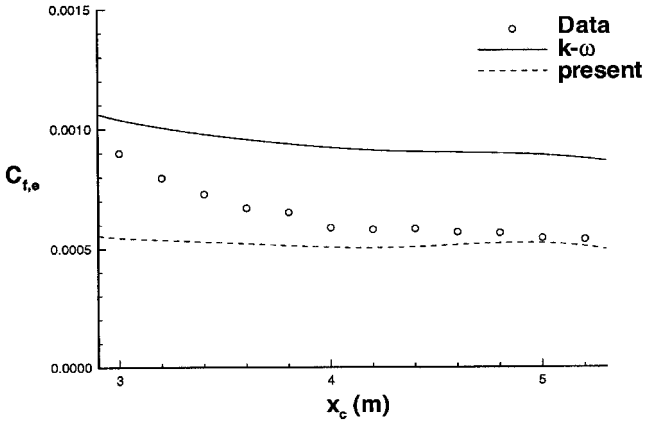

Fig. 1 Comparison of skin friction calculations with experiment.

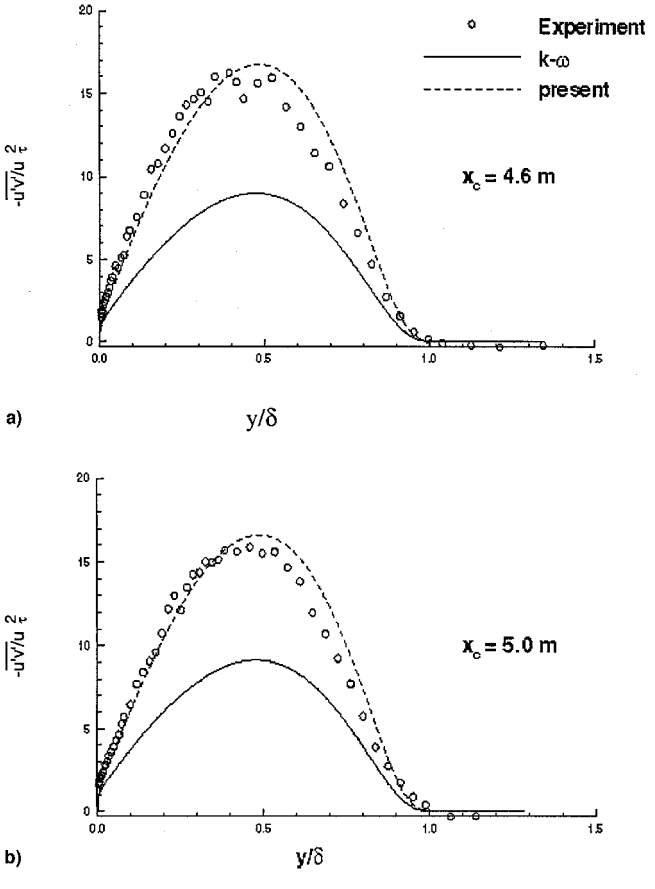

Fig. 2 Comparison of shear-stress profiles with experiment.

Concluding Remarks

This work identifies inadequate diffusion modeling as the cause for the inability to model separated flows or flows on the verge of separation. The results suggest that a new diffusion mechanism needs to be introduced in the k equation to explain observed behavior of turbulent flows in the presence of strong adverse pressure gradients at low speeds. The current modification of the k-ω model with an additional diffusion term based on the pressure gradient showed good agreement with the experiment when strong adverse pressure gradients exist in an incompressible flow.

Acknowledgments

The authors express their sincere appreciation to Per-Age Krogstad for providing them with his digitized data and a copy of Per Egil Skare's Ph.D. dissertation. Computer resources were provided by the North Carolina Supercomputing Center.

References

[1]Skare, P. E., and Krogstad, P. A., "A Turbulent Equilibrium Boundary Layer near Separation," *Journal of Fluid Mechanics*, Vol. 272, Aug. 1994, pp. 319–348.

[2]Krogstad, P. A., and Skare, P. E., "Influence of a Strong Adverse Pressure Gradient on the Turbulent Structure in a Boundary Layer," *Physics of Fluids*, Vol. 7, No. 8, 1995, pp. 2014–2024.

[3]Wilcox, D. C., "Turbulence Modeling in CFD," DCW Industries, Inc., La Canada, CA, 1993.

[4]Stratford, B. S., "The Prediction of Separation of Turbulent Boundary Layers," *Journal of Fluid Mechanics*, Vol. 5, Pt. 1, 1959, pp. 1–16.

[5]Townsend, A. A., "Equilibrium Layers and Wall Turbulence," *Journal of Fluid Mechanics*, Vol. 11, Pt. 1, Aug. 1961, pp. 97–120.

[6]Schubauer, G. B., and Klebanoff, P. S. "Investigation of Separation of the Turbulent Boundary Layer," NACA Rept. 1030, 1951.

[7]Rao, M. S., and Hassan, H. A., "Modeling Turbulence in the Presence of Adverse Pressure Gradients," AIAA Paper 96-2429, June 1996.

[8]Saffman, P. G., "A Model for Inhomogeneous Turbulent Flow," *Proceedings of the Royal Society of London, Series A: Mathematical and Physical Sciences*, Vol. A317, 1970, pp. 417–433.

[9]Harris, J. E., and Blanchard, D. K., "Computer Program for Solving Laminar, Transitional, or Turbulent Compressible Boundary Layer Equations for Two-Dimensional and Axisymmetric Flow," NASA TM 83207, Feb. 1982.

Buckling Analysis of Laminated Fiber-Reinforced Doubly Curved Shallow Shells

Maher N. Bismarck-Nasr*
Instituto Tecnolòǵico de Aeronàutica, São Josè dos Campos, SP, 12228-900, Brazil

I. Introduction

LAMINATED fiber-reinforced composite materials are increasingly used in aeronautical and space vehicles structures as shallow shell structural elements because of their high strength-to-weight ratio. However, their use in the design introduces several complicating factors that are not present in the conventional isotropic material constructions. Such complications are mainly a result of the fiber orientation, the number of layers used, and their stacking sequence. For efficient use, a good understanding of modern materials' construction is needed and their structural stability behavior under various loads and boundary conditions need to be studied. Because of the introduction of the geometric matrix concept by Gallagher and Padlog[1] and Kapur and Hartz,[2] many authors exploited the application of the finite element method for the analysis of linear and nonlinear buckling of plate and shell structures.[3–10] In most of the earlier works on the elastic stability analysis of plates and shells, the total potential energy functional was used for the finite element formulation of the problem. Alternatively, the problem can be formulated using a two-field, variable-modified functional with the transverse displacement w and Airy stress function F as the field variables of the problem. In Ref. 11, starting from Reissner's variational equation for free vibration of thin isotropic cylindrical curved plates, the Euler–Lagrange equations governing the problem and the boundary conditions were obtained. It was shown that the boundary con-

Received May 10, 1997; revision received Oct. 10, 1997; accepted for publication Nov. 9, 1998.

*Professor, Division of Aeronautical Engineering. Member AIAA.

ditions on F are as simple and direct to apply as on w. The formulation was then extended to the buckling analysis,[5,6] to the supersonic flutter,[12] to the problem of stability of cylindrically curved isotropic panels subjected to nonconservative tangential follower forces,[13] and to the aeroelastic analysis of laminated doubly curved shallow shells.[14] The purpose of the present work is to present a two-field, variable-variational formulation, with w and F taken as the field variables, for the elastic stability analysis of fiber-reinforced, doubly curved shallow shells. It is shown that the functional presented has no explicit material bending–extensional coupling terms. These effects appear only in the equivalent material bending stiffness constitutive constants. The solution of the problem is made using a C^1 continuity finite element method. Numerical results are given and the results obtained are discussed and compared with previous solutions, whenever available.

II. Problem Formulation

The variational equation of laminated fiber-reinforced, doubly curved shallow shells, considering the effect of the work done by an initial in-plane prestress load, N^0_x, N^0_y, N^0_{xy} reads[5,6,13,14]

$$\begin{aligned}\delta(\Pi^*) = -\delta\Bigg[&\int_A w\left\{\frac{F_{,xx}}{R_x}+\frac{F_{,yy}}{R_y}\right\}\mathrm{d}A\\ &-\frac{1}{2}\int_A [D^*_{11}w^2_{,xx}+D^*_{22}w^2_{,yy}+2D^*_{12}w_{,xx}w_{,yy}+4D^*_{33}w^2_{,xy}\\ &+4D^*_{13}w_{,xx}w_{,xy}+4D^*_{23}w_{,yy}w_{,xy}]\,\mathrm{d}A\\ &+\frac{1}{2}\int_A [A^*_{22}F^2_{,xx}+A^*_{11}F^2_{,yy}+2A^*_{12}F_{,xx}F_{,yy}+4A^*_{33}F^2_{,xy}\\ &-2A^*_{23}F_{,xx}F_{,xy}-2A^*_{13}F_{,yy}F_{,xy}]\,\mathrm{d}A\\ &-\frac{1}{2}\int_A [N^0_{xx}w^2_{,x}+N^0_{yy}w^2_{,y}+2N^0_{xy}w_{,x}w_{,y}]\,\mathrm{d}A\Bigg]=0\end{aligned}\tag{1}$$

where h is the shell total thickness and, R_x and R_y are the shell radius of curvature in the x and y directions, respectively. The material constitutive constants are obtained from the relation

$$\begin{Bmatrix}\{\boldsymbol{\varepsilon}^0\}\\ \{\boldsymbol{M}\}\end{Bmatrix}=\begin{bmatrix}[A^*] & [-A^{-1}B]\\ [BA^{-1}] & [D^*]\end{bmatrix}\begin{Bmatrix}\{\boldsymbol{N}\}\\ \{\boldsymbol{\kappa}\}\end{Bmatrix}\tag{2}$$

where $\{\boldsymbol{M}\}$ and $\{\boldsymbol{N}\}$ are the stress and moment resultants, $\{\boldsymbol{\varepsilon}^0\}$ and $\{\boldsymbol{\kappa}\}$ are the middle surface strain and curvature vectors, $[A^*]=[A]^{-1}$ and $[D^*]=[D]-[B][A]^{-1}[B]$. The global constitutive matrices, $[A]$, $[B]$, and $[D]$, of the laminated fiber-reinforced composite material are obtained from the laminas properties Q^*_{ij} in the reference coordinates, and can be written as[15,16]

$$A_{ij}=\sum_{k=1}^{n}Q^*_{ij_k}(h_k-h_{k-1}),\qquad B_{ij}=\frac{1}{2}\sum_{k=1}^{n}Q^*_{ij_k}(h_k^2-h_{k-1}^2)$$
$$D_{ij}=\frac{1}{3}\sum_{k=1}^{n}Q^*_{ij_k}(h_k^3-h_{k-1}^3)\tag{3}$$

where h_k is the vectorial distance from the middle surface to the upper surface of the lamina k, and n is the total number of the laminas. Notice that Eq. (1) does not have explicit material bending-in-plane coupling terms, their effects appear only in the equivalent constitutive elements D^*_{ij}. A finite element solution for the problem at hand can be performed, using rectangular elements preserving C^1 continuity, based on the functional given in Eq. (1), using first-order Hermitian polynomials. The element matrices and the boundary conditions are obtained in the same manner as previously reported in Refs. 11–14, and the system finite element equations read

$$[K_{ww}]\{\boldsymbol{w}\}+[K_{wF}]\{\boldsymbol{F}\}+N^0_{xx}[K_{Gxx}]\{\boldsymbol{w}\}+N^0_{yy}[K_{Gyy}]\{\boldsymbol{w}\}+N^0_{xy}[K_{Gxy}]\{\boldsymbol{w}\}=\{\boldsymbol{0}\}\tag{4a}$$

$$[K_{Fw}]\{\boldsymbol{w}\}+[K_{FF}]\{\boldsymbol{F}\}=\{\boldsymbol{0}\}\tag{4b}$$

The degrees of freedom $\{\boldsymbol{F}\}$ can be eliminated using the compatibility equation [Eq. (4b)] and the solution of the problem is reduced to

$$[K_{eq}]\{\boldsymbol{w}\}+N^0_{xx}[K_{Gxx}]\{\boldsymbol{w}\}+N^0_{yy}[K_{Gyy}]\{\boldsymbol{w}\}+N^0_{xy}[K_{Gxy}]\{\boldsymbol{w}\}=\{\boldsymbol{0}\}\tag{5}$$

where $[K_{eq}]=[K_{ww}]-[K_{wF}][K_{FF}]^{-1}[K_{Fw}]$.

III. Numerical Results and Discussion

The first series of calculations presented is for fiber-reinforcement composite material rectangular flat plates with simply supported end conditions on the four edges. This first case has been chosen because it possesses an exact analytical solution for the in-plane buckling loads[16] and, thus, can be used as a test for the precision achieved using the present finite element formulation. The material properties used in the calculations are $E_1=21\times10^6$ psi, $E_2=0.84\times10^6$ psi, $G_{12}=0.42\times10^6$ psi, $\upsilon_{12}=0.25$, and four-layer construction [0/90/90/0]. The layers are of equal thickness and the plate total thickness was 1 in. The calculations were performed for direct in-plane initial stress resultant N^0_{xx}, plate dimension $b=100$ in., and for different plate aspect ratio a/b. All of the present finite element calculations were performed for a mesh of 4×4 elements. In the present example there is no material or geometric bending–stretching coupling, nor bending–twisting coupling, i.e., only the effect of orthotropicity is evidenced. Table 1 shows the results obtained using the present formulation and the comparison with the results of the analytical formula of Ref. 16. From the results of this table, it can be observed that a high precision has been achieved using a 4×4 mesh and, therefore, this mesh size was considered adequate for proceeding to calculations of the critical loads for other configurations. In the second series of calculation the effect of the shell curvature on the critical buckling loads is examined. Three sets of calculations were done. The first set is for cylindrically curved shells, the second set is for paraboloidal shells having $1/R_x=0.5/R_y$, and the third case considered is for spherical shells. All of the calculations were performed for a square planform and the material properties adopted are the same as in the first example. Again, for such properties there is no material bending–stretching coupling, nor bending–twisting coupling, so that the effect of the geometric shell curvature can be directly evidenced. The analyses were performed for

Table 1 Buckling loads[a]

a/b	m,n[b]	Ref. 16	Present
1.0	1,1	7.124	7.127
1.5	1,1	5.318	5.321
2.0	1,1	5.999	6.001
2.5	2,1	5.706	5.733
3.0	2,1	5.318	5.337
3.5	2,1	5.482	5.496
4.0	3,1	5.495	5.592

[a]Critical nondimensional buckling load $\underline{N}^0_{xxcr}=N^0_{xx}b^2/D_{22}\pi^2$, of freely supported [0/90/90/0] rectangular flat plate; $a=100$ in., $h=1$ in., $E_1=21\times10^6$ psi, $E_2=0.84\times10^6$ psi, $G_{12}=0.42\times10^6$ psi, and $\upsilon_{12}=0.25$.
[b]m,n are number of half-waves in x and y directions respectively.

direct, shear, and equal direct biaxial combined critical buckling loads. The results of the analyses are given in Table 2 for various shell curvatures. From these results it can be concluded that the curvature effect is always stabilizing in the sense of increasing the critical buckling load. In the next series of calculations the effect of the boundary conditions on the critical buckling loads is examined. Only results of spherically curved shallow shells having square planform are presented. The analyses were performed for the same material properties as in the previous examples. The results of the calculations for the simply supported and clamped cases are given in Table 3. The results of the freely supported case have already been calculated in Table 2c. From the results obtained it can be concluded that, for the range of the shell curvatures analyzed, the clamped boundary conditions always present higher buckling values compared to the supported conditions. The critical buckling loads, for the simply supported conditions, are always higher than the freely supported end conditions. In the next series of calculations the effect of the material extensional–bending coupling on the critical buckling loads is examined. The freely supported spherical shell with square planform has been taken as the base of the computation. The same material properties of the previous examples is again considered and the calculations were performed for a two-layer construction stacked in the sequence 0/90. The total shell thickness is the same as in the previous examples and is equal to 1 in. The asymmetric layer construction considered here causes a high material extensional–bending coupling that is not present in the previous examples analyzed. The results of the analyses are given in Table 4 and should be compared with the results of Table 2c. From these results it is evident that the material extensional–bending coupling caused by the asymmetric layer construction has a large influence on the critical buckling loads and is always destabilizing, in the sense of decreasing the buckling loads compared to the symmetric layer construction.

Table 2 Shell buckling loads[a]

$1/R_y$	$\underline{N}^{o}_{xxcr}$	$\underline{N}^{o}_{yycr}$	$\underline{N}^{o}_{xycr}$	$\underline{N}^{o}_{xxcr} = \underline{N}^{o}_{yycr}$
a. Critical buckling loads for cylindrical shells, $1/R_x = 0$				
0.000	1.000	0.846	2.327	0.500
0.001	1.201	0.858	2.490	0.600
0.002	1.803	0.893	2.720	0.714
0.005	4.545	1.136	3.264	0.909
0.010	8.021	1.673	4.461	1.506
0.025	20.365	2.692	7.654	2.424
b. Critical buckling loads for paraboloidal shells, $1/R_x = 0.5/R_y$				
0.000	1.000	0.846	2.327	0.500
0.001	1.452	0.951	2.671	0.726
0.002	2.805	1.263	3.168	1.011
0.005	6.845	2.957	4.965	2.662
0.010	14.260	6.365	8.077	5.104
0.025	36.320	16.353	18.041	12.707
c. Critical buckling loads for spherical shells, $1/R_x = 1/R_y$				
0.000	1.000	0.846	2.327	0.500
0.001	1.803	1.136	2.898	0.901
0.002	4.209	2.005	3.812	1.604
0.005	9.036	5.564	6.619	4.493
0.010	17.933	10.862	11.333	8.201
0.025	47.344	28.241	27.006	20.985

[a]Critical buckling loads of freely supported [0/90/90/0] rectangular shallow shells; $a = b = 100$ in., $h = 1$ in., $E_1 = 21 \times 10^6$ psi, $E_2 = 0.84 \times 10^6$ psi, $G_{12} = 0.42 \times 10^6$ psi, and $v_{12} = 0.25$. The critical loads are nondimensionalized for the flat-plate value, $N^{o}_{xxcr} = 1973.57$.

Table 3 Shell buckling loads[a]

$1/R_y$	$\underline{N}^{o}_{xxcr}$	$\underline{N}^{o}_{yycr}$	$\underline{N}^{o}_{xycr}$	$\underline{N}^{o}_{xxcr} = \underline{N}^{o}_{yycr}$
a. Critical buckling loads for simply supported spherical shells, $1/R_x = 1/R_y$				
0.000	1.000	0.846	2.327	0.500
0.001	4.399	2.011	3.554	1.629
0.002	5.519	3.805	4.632	2.604
0.005	12.093	6.792	7.292	5.123
0.010	21.502	12.513	11.962	9.213
0.025	49.503	30.350	27.546	22.345
b. Critical buckling loads for clamped spherical shells, $1/R_x = 1/R_y$				
0.000	6.739	2.106	4.361	1.676
0.001	7.600	2.854	4.925	2.335
0.002	9.178	4.673	5.928	3.574
0.005	14.899	8.215	8.607	5.978
0.010	23.680	14.251	13.484	10.401
0.025	56.696	31.438	31.677	24.250

[a]Critical buckling loads of simply supported and clamped [0/90/90/0] rectangular shallow spherical shells; $a = b = 100$ in., $h = 1$ in., $E_1 = 21 \times 10^6$ psi, $E_2 = 0.84 \times 10^6$ psi, $G_{12} = 0.42 \times 10^6$ psi, and $v_{12} = 0.25$. The critical loads are nondimensionalized for the simply supported flat-plate value, $N^{o}_{xxcr} = 1973.57$.

Table 4 Shell buckling loads[a]

$1/R_y$	$\underline{N}^{o}_{xxcr}$	$\underline{N}^{o}_{yycr}$	$\underline{N}^{o}_{xycr}$	$\underline{N}^{o}_{xxcr} = \underline{N}^{o}_{yycr}$
Critical buckling loads for simply supported spherical shells, $1/R_x = 1/R_y$				
0.000	0.406	0.406	0.983	0.203
0.001	1.070	1.070	1.500	0.604
0.002	1.939	1.939	2.186	1.217
0.005	4.667	4.667	4.149	2.983
0.010	9.992	9.992	7.461	6.328
0.025	25.995	25.995	19.091	15.761

[a]Critical buckling loads of freely supported [0/90] rectangular shallow spherical shells; $a = b = 100$ in., $h = 1$ in., $E_1 = 21 \times 10^6$ psi, $E_2 = 0.84 \times 10^6$ psi, $G_{12} = 0.42 \times 10^6$ psi, and $v_{12} = 0.25$. The critical loads are nondimensionalized for the simply supported flat-plate value for the [0/90/90/0] construction, $N^{o}_{xxcr} = 1973.57$.

Acknowledgment

Grant 300954/91-3 of CNPq (Brazil) conceded to the author during the preparation of this work is gratefully acknowledged.

References

[1]Gallagher, R. H., and Padlog, J., "Discrete Element Approach to Structural Stability Analysis," *AIAA Journal*, Vol. 1, No. 6, 1963, pp. 1437–1439.

[2]Kapur, K. K., and Hartz, J., "Stability of Plates Using the Finite Element Method," *Journal of Engineering Mechanical Division*, Vol. 92, No. EM2, 1966, pp. 177–195.

[3]Carson, W. G., and Newton, R. E., "Plate Buckling Analysis Using a Fully Compatible Finite Element," *AIAA Journal*, Vol. 7, No. 3, 1969, pp. 527–529.

[4]Pifko, A., and Isakson, G., "A Finite Element Method for the Plastic Buckling Analysis of Plates," *AIAA Journal*, Vol. 7, No. 10, 1969, pp. 1950–1957.

[5]Bismarck-Nasr, M. N., "Buckling Analysis of Cylindrically Curved Panels Based on a Two Field Variable Variational Principle," *International Journal of Computers and Structures*, Vol. 51, No. 4, 1994, pp. 453–457.

[6]Bismarck-Nasr, M. N., "Analysis of Cylindrically Curved Panels Based on a Two Field Variable Variational Principle," *Applied Mechanics Reviews*. Vol. 46, No. 11, Pt. 2, 1993, pp. 571–578.

[7]Cook, R. D., *Concepts and Applications of Finite Element Analysis*, Wiley, New York, 1974.

[8]Nath, B., *Fundamentals of Finite Elements for Engineers*, The Athlone Press of the Univ. of London, 1974.

[9]Gallagher, R. H., *Finite Element Analysis, Fundamentals*, Prentice–Hall, Englewood Cliffs, NJ, 1975.

[10]Bismarck-Nasr, M. N., *Finite Elements in Applied Mechanics*, Abaetè Gràfica, São Paulo, Brazil, 1993.

[11]Bismarck-Nasr, M. N., "On Vibration of Thin Cylindrically Curved Panels," *Proceedings of the 3rd Pan American Congress of Applied Mechanics, PACAM III* (São Paulo, Brazil), edited by D. T. Mook and D. L. Zagottis, Univ. of São Paulo, SP, Brazil, 1993, pp. 696–699.

[12]Bismarck-Nasr, M. N., "Supersonic Panel Flutter Analysis of Shallow Shells," *AIAA Journal*, Vol. 31, No. 7, 1993, pp. 1349–1351.
[13]Bismarck-Nasr, M. N., "Dynamic Stability of Shallow Shells Subjected to Follower Forces," *AIAA Journal*, Vol. 33, No. 2, 1995, pp. 355–360.
[14]Bismarck-Nasr, M. N., "Aeroelasticity of Laminated Fibre-Reinforced Doubly Curved Shallow Shells," *AIAA Journal*, Vol. 36, No. 4, 1998, pp. 661–663.
[15]Reissner, E., and Stavsky, Y., "Bending and Stretching of Certain Types of Heterogeneous Aleotropic Elastic Plates," *Journal of Applied Mechanics*, Vol. 26, No. 9, 1961, pp. 402–408.
[16]Jones, R. M., *Mechanics of Composite Materials*, McGraw–Hill—Kogakusha Ltd., Tokyo, 1975.

Aeroelastic Design Optimization with Experimental Verification

Jakob Kuttenkeuler* and Ulf Ringertz†
Royal Institute of Technology, Stockholm S-100 44, Sweden

Introduction

THE optimal design of aircraft structures subject to aeroelastic stability constraints, so-called aeroelastic tailoring, is not new. Early studies involved using the anisotropic properties of laminated wood or plywood structures to tailor the structural response caused by aerodynamic forces.[1] The development of finite element structural analysis, potential flow panel methods, and numerical optimization made it possible to solve quite complex aeroelastic tailoring problems. Important early contributions were done by Haftka and Yates[2] and Wilkinson et al.[3] Use of modern composite materials have further improved the possibilities in tailoring the structural response under aerodynamic loads for performance benefits. The X-29 demonstrator is perhaps the most well-known example.[4]

Because aeroelastic tailoring is true multidisciplinary analysis and optimization, there is an obvious risk that modeling errors in each discipline multiply when the different models are combined in an optimization process. Evaluation of the aeroelastic stability constraints involves the solution of nonlinear eigenvalue problems with unsymmetric and complex matrices. It is well known that this type of eigenvalue constraint is not differentiable with respect to design changes and may also lead to discontinuities in other problem parameters such as flutter speed.[5–7]

The purpose of the present paper is to demonstrate the accuracy of the most common analysis methods used in aeroelastic tailoring for predicting aeroelastic stability by comparing numerical results with wind-tunnel experiments. The particular interest is to closely investigate design points in the neighborhood of optimal designs where discontinuities in flutter speed with respect to design changes appear. The use of optimal design methods tends to increase the likelihood of obtaining structures that, at least in theory, are extremely sensitive to small perturbations and imperfections in material properties, boundary conditions, and aerodynamic flow models.

Model Problem

The model design problem was chosen as a thin composite wing with orthotropic material properties. The design variables were the orientation of the material and the size of a number of concentrated masses used for mass balancing. There are several advantages with using a polymer composite wing. The composite material is superior in withstanding large strains, e.g., when subject to flutter, without permanent deformations caused by yielding and it offers many possibilities for aeroelastic tailoring.

The wing geometry and material were selected on the basis of tunnel performance and geometry. The configuration was chosen to be of relevant size, materialize a suitable critical speed, and to not have a divergence instability. A 15-deg swept configuration with 1200-mm span, 200-mm root chord, and 100-mm tip chord was chosen. Planform and definition of the coordinate system are shown in Fig. 1, where γ defines the sweep angle and θ defines the orientation of the 0-deg laminate axis. The nominal wing thickness was 2.0 mm.

All wings were cut from prefabricated, epoxy-impregnated woven glass-fiber laminates with the objective to be identical with respect to planform and thickness. The lay-up was orthotropic with all fibers aligned parallel to either the 0- or 90-deg axis of the laminate. Because of differences in the weave structure between the warp and weft yarns, both the Young's moduli and the bending stiffnesses varied between the two main axes. The 0-deg axis was defined here as the axis of highest stiffness.

The dominating elastic material properties in the present aeroelastic problem are the plate stiffnesses, D_{ij}. Several different mechanical tests were performed to determine reliable and representative material properties. After some consideration it was decided to consistently use the results from a vibration technique[8,9] that is able to measure all D_{ij} of a specimen in one single test. The advantage of the method was notable, particularly because it is quite difficult to measure, e.g., D_{66} using standard test methods.

The method of Frederiksen[8,9] uses experimentally determined eigenfrequencies of rectangular specimen plates to match numerical results where the elastic lamina properties are used as variables in an optimization process. An error function describing the difference between the experiments and the numerical results is minimized. The experiments showed variations in elastic properties, primarily because of laminate thickness variations, but likely also because of local deviations in lamina orientations. Table 1 shows representative plate stiffnesses for the thinnest, average, and thickest wing in the investigation. All material data are given in the global x–y coordinate system defined in Fig. 1.

The out-of-plane shear moduli G_{13} and G_{23} were also needed because the Mindlin plate differential equations[10] were used in

Table 1 Representative material properties for the glass-fiber/epoxy laminates

Thickness, mm	Density, kg/m^3	D_{11}, Nm	D_{22}, Nm	D_{12}, Nm	D_{66}, Nm
1.95	1978	18.1	16.4	2.84	3.76
2.06	1929	20.0	18.2	3.19	4.23
2.14	1916	21.8	19.5	3.31	4.48

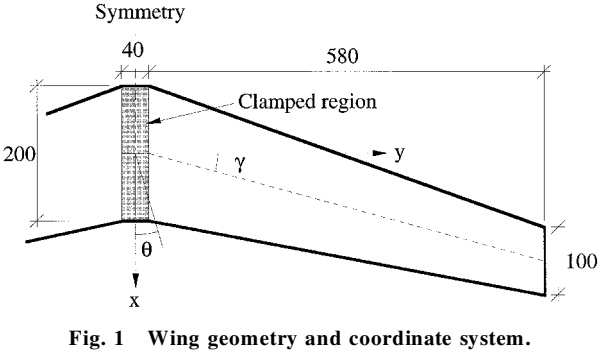

Fig. 1 Wing geometry and coordinate system.

Received Jan. 15, 1997; revision received Nov. 15, 1997; accepted for publication Jan. 9, 1998.

*Ph.D. Student, Department of Aeronautics. E-mail: jakob@flyg.kth.se.
†Professor, Department of Aeronautics. E-mail: rzu@flyg.kth.se. Member AIAA.